Fourier-domain biophotoacoustic subsurface depth selective amplitude and phase imaging of turbid phantoms and biological tissue

Sergey A. Telenkov
Andreas Mandelis*
Center for Advanced Diffusion-Wave Technologies
University of Toronto
Department of Mechanical and Industrial Engineering
Toronto, Ontario, M5S 3G8 Canada

Abstract. A novel photothermoacoustic imaging modality utilizing a frequency-swept (chirped) intensity-modulated laser source and coherent frequency domain signal processing ("biophotoacoustics") was introduced for noninvasive imaging of biological tissues. The developed frequency-domain imaging system takes advantage of linear frequency modulation waveforms to relate depth of tissue chromophores to the frequency spectrum of the detected acoustic response and of a narrow signal detection bandwidth to improve signal-to-noise ratio (SNR). Application of frequency-domain photothermoacoustic (FD-PTA) imaging was demonstrated using turbid phantoms and *ex-vivo* specimens of chicken breast with embedded absorbing inclusions simulating tumors. [DOI: 10.1117/1.2337290]

Keywords: biophotoacoustics; biomedical optics; imaging systems; thermo-optics; Fourier transforms; tissue.

Paper 05370R received Dec. 7, 2005; revised manuscript received Apr. 7, 2006; accepted for publication Apr. 10, 2006; published online Aug. 23, 2006.

1 Introduction

Photoacoustic imaging [or photothermoacoustic (PTA) to emphasize the operating energy conversion mechanism] of biological tissues has received significant attention in recent years due to its ability to detect optical inhomogeneities in tissues with submillimeter spatial resolution at depths of several centimeters. Particular interest in biomedical photoacoustics has been motivated by the promise shown in recent experiments exploring noninvasive imaging of breast and brain tumors.[1–3] Detection of laser-induced acoustic waves reveals localized increase in absorption coefficient, which may be a result of tissue angiogenesis (excessive vascularization) associated with rapid tumor growth. Inasmuch as the PTA technique is sensitive to optical contrast in biological tissues, it can be utilized as a diagnostic tool to provide supplementary information to well-established imaging modalities such as X-ray mammography and ultrasonography.

The mainstream of biomedical photoacoustics is based almost entirely on pulsed laser excitation and time-resolved measurements of acoustic transients to determine position and optical properties of subsurface tissue chromophores.[4,5] A number of important factors favor the use of pulsed laser sources for generating acoustic transients. Specifically, the amplitude of the acoustic pressure response is relatively high; the temporal profile of PTA signals in response to short (ns) laser pulse exposure is related to the distribution of optical energy in the targeted tissue; and the depth of acoustic sources can be straightforwardly determined from time-of-flight measurements. The most sophisticated implementations of pulsed PTA technology include systems with arrays of ultrasonic sensors,[6] scanning mechanisms for acoustic detection in a large solid angle,[7] and advanced three-dimensional tomographic algorithms to reconstruct spatial distribution of acoustic sources.[8,9] Despite promising results demonstrated in experiments with pulsed PTA systems, there are certain difficulties one must address when using the pulsed PTA technique for biomedical imaging. First, time-resolved measurements require wide bandwidth (0.05–10 MHz) and very sensitive ultrasonic transducers to provide sufficient signal-to-noise ratio (SNR) across the broad detection bandwidth. Next, implementation of sophisticated signal conditioning routines is required prior to the application of tomographic reconstruction algorithms to avoid artifacts in the resulting images. Conditioning is especially important in back-propagation detection when only one surface is available for laser excitation and acoustic wave detection. In this configuration a weak PTA signal from subsurface chromophores can be accompanied by a strong acoustic response from superficial tissue layers receiving a significant portion of the optical energy. Although detection of subsurface chromophores as deep as 5–6 cm was reported previously in phantom experiments,[1] the relatively low SNR of the pulsed method poses significant problems for artifact-free image reconstructions. Use of high peak-power pulsed laser irradiation may improve the image quality of deeply embedded inhomogeneities. However, safety standards require limiting laser exposure at levels $<100\ \mathrm{mJ/cm^2}$. Additionally, the lack of reliable and inexpensive ns laser sources tunable in the near-IR spectral range makes it difficult to tailor

Currently at Imaging Diagnostic Systems, Inc., Plantation, Florida.
*Address all correspondence to Andreas Mandelis, Mechanical & Industrial Engineering, Univ. of Toronto, 5 King's College Road, Toronto, ON M5S 3G8 Canada; Tel: 416/987-5106; Fax: 416/978-5106; E-mail: mandelis@mie.utoronto.ca

1083-3668/2006/11(4)/044006/10/$22.00 © 2006 SPIE

the pulsed PTA technique to specific tissue chromophores.

In the present paper, we report the development of frequency (or Fourier-) domain (FD) biophotoacoustics, an alternative approach based on a linear frequency modulated (LFM) or chirped laser source and Fourier-spectrum signal acquisition and processing methodologies. The term *biophotoacoustics* is introduced to indicate the fundamentally photonic nature of biological FD-PTA signals, especially the need for analytical and numerical techniques based on diffuse photon density-wave propagation in tissue for quantitative analysis of data, with the acoustic wave acting as a carrier of optical information and possibly as an amplifier of optical contrast[10,11] through the dependence of the thermal and acoustic properties of tissue on the degree of tissue vascularization. Advantages of frequency domain biophotoacoustics over pulsed excitation include (1) the tissue is exposed to much lower laser fluence, (2) a coherent data processing algorithm can be utilized to increase SNR significantly and offset reduction of acoustic pressure amplitude, (3) a direct relationship between time-delay of acoustic response and depth of tissue chromophores can be recovered using linear frequency sweeps and heterodyne signal processing, (4) a wide selection of inexpensive diode laser sources is available in the near-IR, which makes possible the design of compact devices tailored to specific biochemical composition of tissue, and (5) a potentially superior signal-to-noise ratio.

Historically, frequency domain PTA methods with periodic single-frequency modulated laser sources have not been actively pursued in imaging applications of turbid media because the amplitude of the laser-induced acoustic waves is typically several orders of magnitude lower than in pulsed PTA systems. Moreover, measurements at a single modulation frequency and coherent signal detection fail to provide unambiguous and/or wide depth information because typical acoustic wavelengths in the megahertz frequency range are less than 1 mm. Therefore, an alternative (hybrid) scheme of PTA generation and detection must be introduced to take advantage of both the high SNR of frequency domain techniques and the simplicity of time-of-flight measurements typical to pulsed methods. Application of waveforms with linear frequency sweeps helps to avoid ambiguity in depth measurements and dramatically increases the attainable depth range while exhibiting substantial SNR increase and background signal suppression using correlation or heterodyne demodulation methods for signal detection. The concept of using linear frequency modulation (LFM) waveforms for depth profilometry finds numerous similarities in radar technology.[12] In order to increase radar detection range and avoid generation of high peak-power bursts of radiowaves, a much longer pulse with LFM coding is used. This method of signal generation does not result in deterioration of spatial resolution because the returning echo is compressed into a narrow spike using a matched filter at the signal processing stage.

Another example where frequency-swept signals have been successfully utilized for depth profilometry and imaging is Fourier-domain optical coherence tomography (FD-OCT).[13,14] It has been shown[15,16] that spectral measurements employed by FD-OCT with a swept laser source demonstrate concrete advantages over the conventional time-domain technique in terms of SNR. Similar SNR advantages are expected in the case of FD-PTA. The distinguishing difference between purely optical or ultrasonic methodologies based on detection of echo signals and laser biophotoacoustics is that the latter relies on conversion of optical energy into thermoelastic pressure waves, which are largely immune to optical turbidity. This low sensitivity of the FD-PTA technique to strong light scattering, which poses serious difficulties to purely optical imaging modalities, is a unique asset for increasing probe depth in tissues. Acoustic wave attenuation in the 1–5 MHz range is relatively small, allowing the examination of tissue optical properties at several centimeters. Our results demonstrate that frequency domain biophotoacoustics can be successfully utilized for depth profilometry and depth-selective imaging of biological tissues.

2 FD-PTA Imaging System and Signal Processing Algorithms

A schematic diagram of our imaging system with a linear frequency modulated laser source is shown in Fig. 1. In the present implementation of biophotoacoustics we used intensity-modulated IR radiation emitted by a CW laser source at 1064 nm (IPG Photonics, MA). The choice of laser source was based on two factors: relatively deep penetration in tissue and sufficient output power in order to use an acousto-optic modulator (AOM) (Neos Technologies, FL) for intensity modulation in the MHz frequency range. The LFM chirps with duration of 1 ms and the frequency sweep range from 1 MHz to 5 MHz were generated continuously by a function generator (DS345, Stanford Research Systems, CA). Synchronization of the modulation chirps and data acquisition hardware was controlled by the trigger pulses from a delay generator (DG535, Stanford Research Systems, CA). To detect the PTA response, we used a focused ultrasonic transducer (Panametrics, V382) with maximum sensitivity at 3.5 MHz and focal distance of 25.4 mm. Test samples were immersed in a water container to ensure acoustic coupling, and a focused laser beam (diameter $\sim$1 mm) irradiated the sample surface at a small angle ($\sim 10°$). The power of the modulated laser beam entering the water was varied in the range of 100–400 mW. The water container was mounted on an XY-stage and was driven by step motors either along a straight line to record 2-D "slice" images or over a specified surface area for 3-D volume imaging. For signal acquisition in the FD-PTA system, we used a high-speed dual-channel analog-to-digital converter (ADC) (PCI-5122, National Instruments, TX) capable of 100 MHz maximum sampling rate and controlled via a graphical user interface designed in the LabView environment. A trigger pulse from the delay generator starts modulation chirp generation and simultaneous data acquisition through the two channels of the ADC board. One channel of the ADC records a copy of the modulation chirp and another channel receives the output of the preamplifier connected to the ultrasonic transducer. In each triggering event, a data sequence 30–50 ms long is recorded and run through a data processing algorithm. Digital signal processing and image visualization are implemented as software modules that operate with frequency-modulated waveforms. The main advantage of chirped modulation in the FD-PTA system is the ability to use coherent processing methods to increase SNR and to preserve the relationship between the depth of acoustic sources, z, and the delay time, τ, of acoustic wave arrival: z

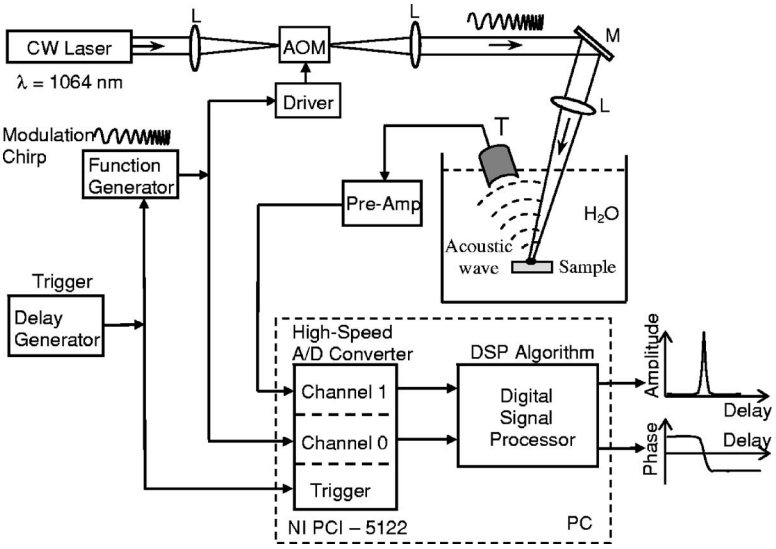

Fig. 1 Schematic diagram of the FD-PTA imaging system with a frequency-swept laser source. AOM—acousto-optic modulator, L—lenses, M—mirror, T—ultrasonic transducer.

$=c_a\tau$, where c_a is the speed of sound in tissue.

Two methodologies were employed for processing the LFM responses received by the ultrasonic transducer. One approach is similar to that utilized in radar applications and is based on correlation measurements (or matched filter compression) of the received PTA signal and of a reference LFM waveform with known characteristics. The other approach uses heterodyne mixing to relate the frequency (Fourier) spectrum of the down-shifted signal to the depth of acoustic sources. Subsequently, a single frequency coherent (lock-in) detection technique with high SNR was applied to analyze the spectrum and reconstruct the depth distribution of tissue chromophores. Since both signal processing methodologies were utilized in our experiments, a description of the basic physical signal generation principles is given ahead in greater detail.

2.1 *Correlation Processing (Matched Filter Compression)*

Matched filter detection of a signal $s(t)$ buried in white noise is based on the fact that the highest SNR is achieved at the time $t=t_0$ if the filter frequency response $H(\omega)$ is equal to the complex conjugate of the signal spectrum:[17]

$$H(\omega) = S^*(\omega)e^{-i\omega t_0} \tag{1}$$

The output of the filter with spectral response (1) is given by

$$s_{\text{out}}(t) = \frac{1}{2\pi}\int_{-\infty}^{\infty} S(\omega)H(\omega)e^{i\omega t}d\omega = \frac{1}{2\pi}\int_{-\infty}^{\infty} |S(\omega)|^2 e^{i\omega(t-t_0)}d\omega$$

$$= B_s(t-t_0) \tag{2}$$

where $B_s(t-t_0)$ is the correlation function of signal $s(t)$. The matched filter adjusts phases of individual frequency components, which results in a high magnitude and narrow spike at the time $t=t_0$. When an LFM signal is used for laser source modulation, the received acoustic response is correlated with a replica of the modulation chirp to compute $B(\tau)$, where $\tau=t-t_0$. An important parameter of LFM signals is the time-bandwidth product $m=2f_dT_s$, where T_s is the chirp duration and f_d is the frequency deviation in a chirp from the central f_0 (i.e., $f_0\pm f_d$). The value of m defines the result of correlation processing given by Eq. (2). The output of matched filter processing is a compressed sinc-function envelope with a harmonic filling at the central frequency f_0. The main narrow peak occurs at the time $t=t_0$ when the reference chirp is coherent with a delayed acoustic chirp buried in much stronger white noise. The theoretical ratio of the matched filter output amplitude to that of input chirp is $|s_{\text{out}}|/|s_{\text{in}}|=m^{1/2}$, and the signal compression ratio is $T_s/T_{\text{out}}=m$. The instantaneous amplitude increase can be significant for high values of m. In our experiments, the chirp bandwidth was $\Delta f=4$ MHz and $T_s=1$ ms. Therefore, the time-bandwidth product was $m=4000$. Practical implementation of matched filter processing is shown in Fig. 2(a). This algorithm takes advantage of high-speed FFT routines to compute the correlation function in the Fourier domain and transform back to time domain using the inverse FFT. Additionally, frequency weighting is applied to the product of spectra to reduce side lobes of the time-domain correlation signal.

2.2 *Heterodyne Mixing with Coherent Detection*

The second approach is based on heterodyne mixing of LFM waveforms and coherent detection of the down-shifted signal at the single frequency specified by an internally generated reference signal. In this method, the depth of tissue chromophores generating a chirped PTA response is mapped into the frequency spectrum of the heterodyned signals. The principle of heterodyne mixing is shown in Fig. 2(b). The dual channel ADC records simultaneously a copy of the modulation chirp $r(t)=\exp[i2\pi(f_0+\beta t)t]$, where β is the frequency sweep rate, and of the chirped PTA response $s(t)$ received by the ultrasonic transducer. Assuming that a tissue sample contains a discrete chromophore at depth z, the PTA signal detected by the transducer contains the chirp $f(t)=f_0+\beta(t-t_0)$

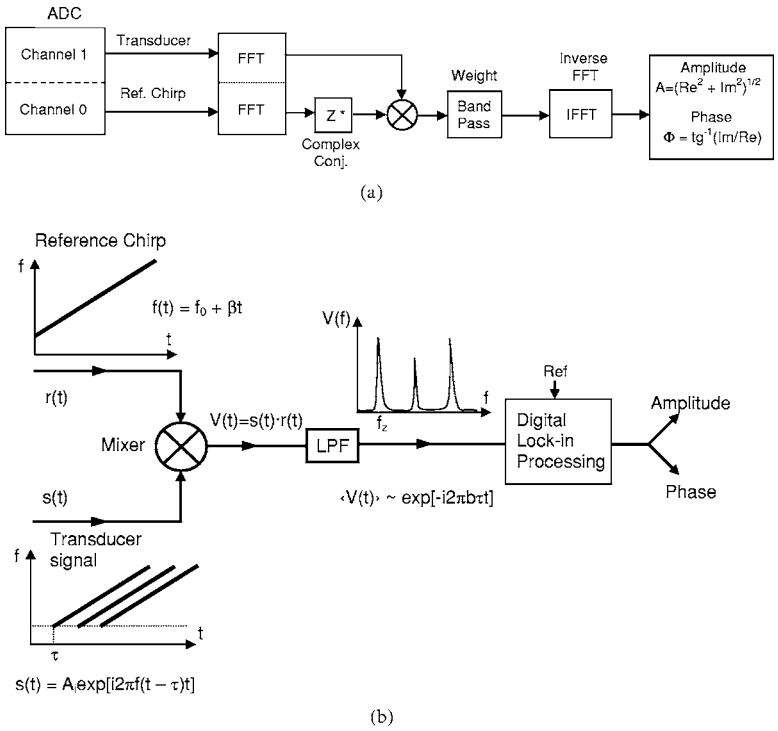

Fig. 2 (a) Block-diagram of data flow in a correlation signal processing algorithm; (b) processing of LFM signals using heterodyne mixing with a narrow-band coherent detection.

delayed by the time $t_0=z/c_a$. The delayed PTA response can be written as:[10]

$$s(t)=A_s\exp\left\{i2\pi\left[(f_0-\beta t_0)t+\beta\frac{t^2}{2}\right]\right\} \tag{3}$$

where A_s is the complex amplitude and is assumed to be a constant within the chirp bandwidth. Computing the product $s(t)\cdot r(t)$ and removing the sum frequency components using a low-pass filter, we have for the down-shifted signal $V(t)$:

$$V(t)=\langle s(t)\cdot r(t)\rangle\propto A_s\exp(i2\pi\beta t_0 t)=A_s\exp\left(i2\pi\beta\frac{z}{c_a}t\right) \tag{4}$$

Equation (4) shows that for the specific depth z of a PTA source, the signal $V(t)$ contains the frequency component $f_z=\beta z/c_a$. Therefore, heterodyne mixing provides a direct relationship between the spectrum of the down-shifted signal and the depth of photoacoustic sources. Measurements of the spectral content [Eq. (4)] with high SNR can be conducted using a lock-in detection algorithm with a reference signal synthesized internally at the predetermined frequency f_r. Since coherent lock-in processing effectively suppresses all signals at the frequencies $f\neq f_r$, setting the reference frequency f_r is equivalent to selecting a specific depth for PTA imaging. Combination of this detection method with a focused ultrasonic transducer allows for implementing a photothermoacoustic analogy of confocal imaging when the signal is detected only from the small volume at the focal spot of the transducer (see Sec. 4).

To characterize system response and performance of the signal processing algorithm, the autocorrelation function of a noise-free chirp signal delayed by 30 μs was recorded, which represents an ideal case scenario of FD-PTA detection. Plots in Figs. 3(a) and 3(b) show amplitude and phase of the correlation function computed using real and imaginary parts of $B(\tau)$. The peak position indicates signal arrival and the linear phase $\varphi=-2\pi f_0 t$ is due to the harmonic component ($f_0=3$ MHz) of the correlation function. The peak FWHM is 0.5 μs and defines the axial resolution, which corresponds to 0.75 mm for speed of sound $c_a=1.5\times10^5$ cm/s.

3 Results and Discussion

To demonstrate the feasibility of noninvasive FD-PTA imaging, a series of experiments were conducted with turbid phantoms prepared from an insoluble in water polyvinyl chloride plastisol (PVCP)[18] as well as with *ex-vivo* tissue specimens (chicken breast) containing embedded light-absorbing plastisol inclusions to simulate subsurface tumors. The test samples were positioned in a water bath at the distance of 25.4 mm from the immersed focused transducer. To prevent absorption of the surrounding water by chicken breast tissue, those samples were wrapped in a transparent plastic film. Horizontal translation of samples enabled recording 2-D slice images or 3-D volumetric data arrays.

An example of depth-profilometric measurement at a single spatial point conducted with a light-absorbing plastisol sample (absorption coefficient $\mu_a=1$ cm^{-1}) is shown in Fig. 3(c). This plot depicts the correlation function amplitude of the PTA response following absorption of LFM optical exci-

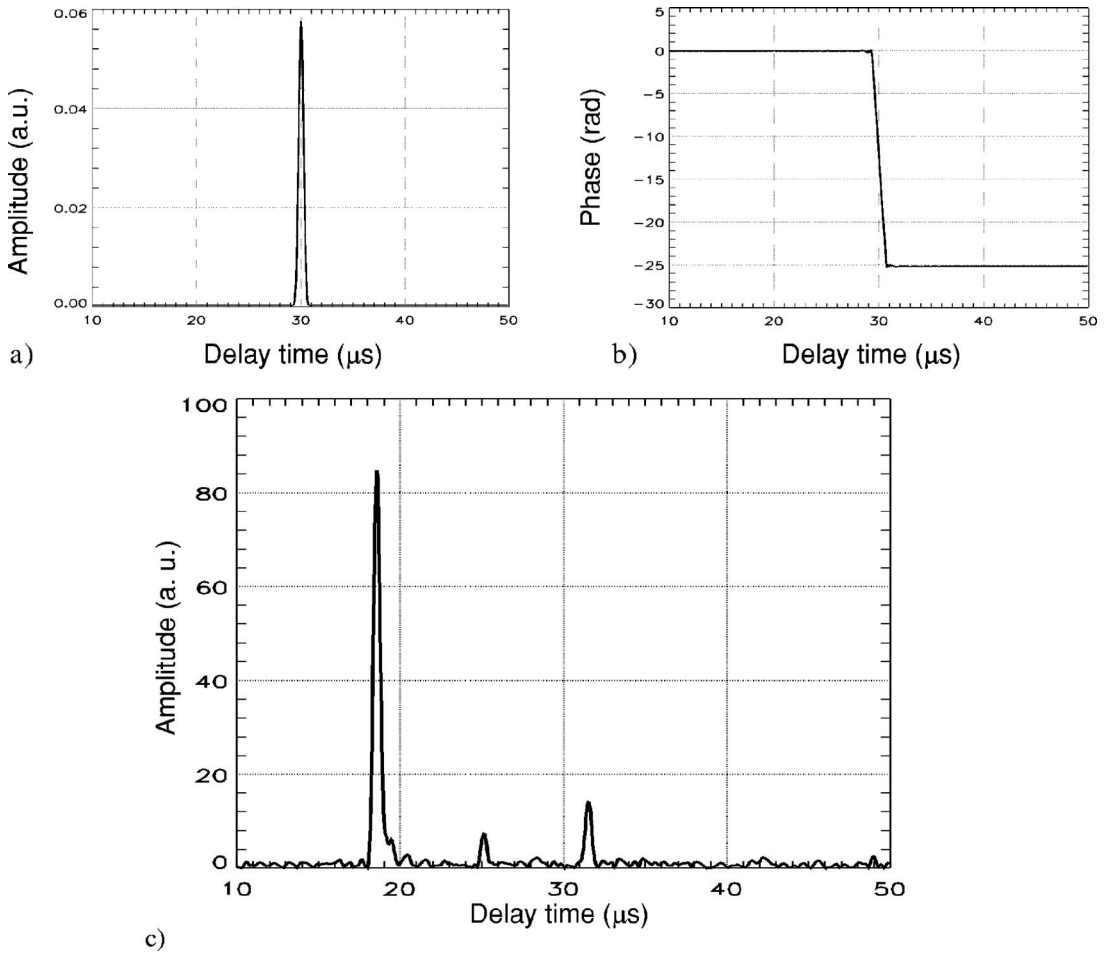

Fig. 3 Amplitude (a) and phase (b) of a correlation function recorded by the FD-PTA system for a noise-free LFM signal delayed by 30 μs. Depth-profilometric measurement (c) of the PTA response from a light-absorbing plastisol phantom (μ_a=1 cm^{-1}).

tation in a 9.5-mm-thick sample. Characteristic features observed in the plot include the first strong peak at 18.5 μs, which corresponds to the PTA signal generated at the sample surface; the second, significantly weaker, peak is the acoustic wave excited on the back interface by the light transmitted through the sample thickness[10] (speed of sound in PVCP is $c_a = 1.4 \times 10^5$ cm/s); and the final (third) peak delayed by 32 μs is the signal due to reflection of acoustic waves generated at the front surface after a round-trip travel through the sample thickness. The magnitude of the first peak is proportional to the laser irradiation intensity and the sample absorption coefficient. The peak FWHM is consistent with the autocorrelation function shown in Fig. 3(a). The noise floor of the data shown in Fig. 3(c) is approximately −32.5 dB.

FD-PTA imaging of subsurface chromophores was studied with turbid phantoms, the optical properties of which were varied by mixing absorbing and scattering constituents at different concentrations. Results shown in Fig. 4 were obtained for a phantom with homogeneous absorption and scattering (absorption and reduced scattering coefficients were $\mu_a = 0.5$ cm^{-1} and $\mu_s' = 1.3$ cm^{-1}, respectively), containing a rectangular-shaped inclusion with increased absorption coefficient (μ_a=4.2 cm^{-1}). Figure 4(a) shows the sample internal structure and the directions of laser-beam scans over a 12 $\times$ 12 mm^2 area. The rectangular inclusion was positioned 6 mm below the top surface. Additionally, a narrow air gap was artificially created immediately under the inclusion to introduce a discontinuity in mechanical properties. A two-dimensional FD-PTA image recorded following a 12-mm line scan and correlation data processing is shown in Fig. 4(b). The vertical axis in the image is labeled in the units of reference signal delay time, τ, which can be simply converted into depth using the speed of sound in water (1.5×10^5 cm/s) and in plastisol (1.4×10^5 cm/s).[18] In Fig. 4(b), the phantom occupies the range of delay times from 18.7 μs to 33 μs. Laser-induced acoustic sources appear in the image as discrete bright lines corresponding to delay time τ when the received acoustic signal is coherent with the reference chirp yielding a correlation function peak. The sample top surface appears as a continuous line positioned at the delay of 18.7 μs. At the beginning of the scan only this signal is present. However, when the scanning laser beam reaches the edge of the inclusion, a strong signal appears at 23 μs along with a weaker one at the delay time of 45.7 μs, which corresponds to an acoustic echo reflected from the sample back surface. Discontinuities of mechanical properties (subsurface air gap) produce strong acoustic reflections that appear on amplitude images as false deep sources. This effect is similar to standard

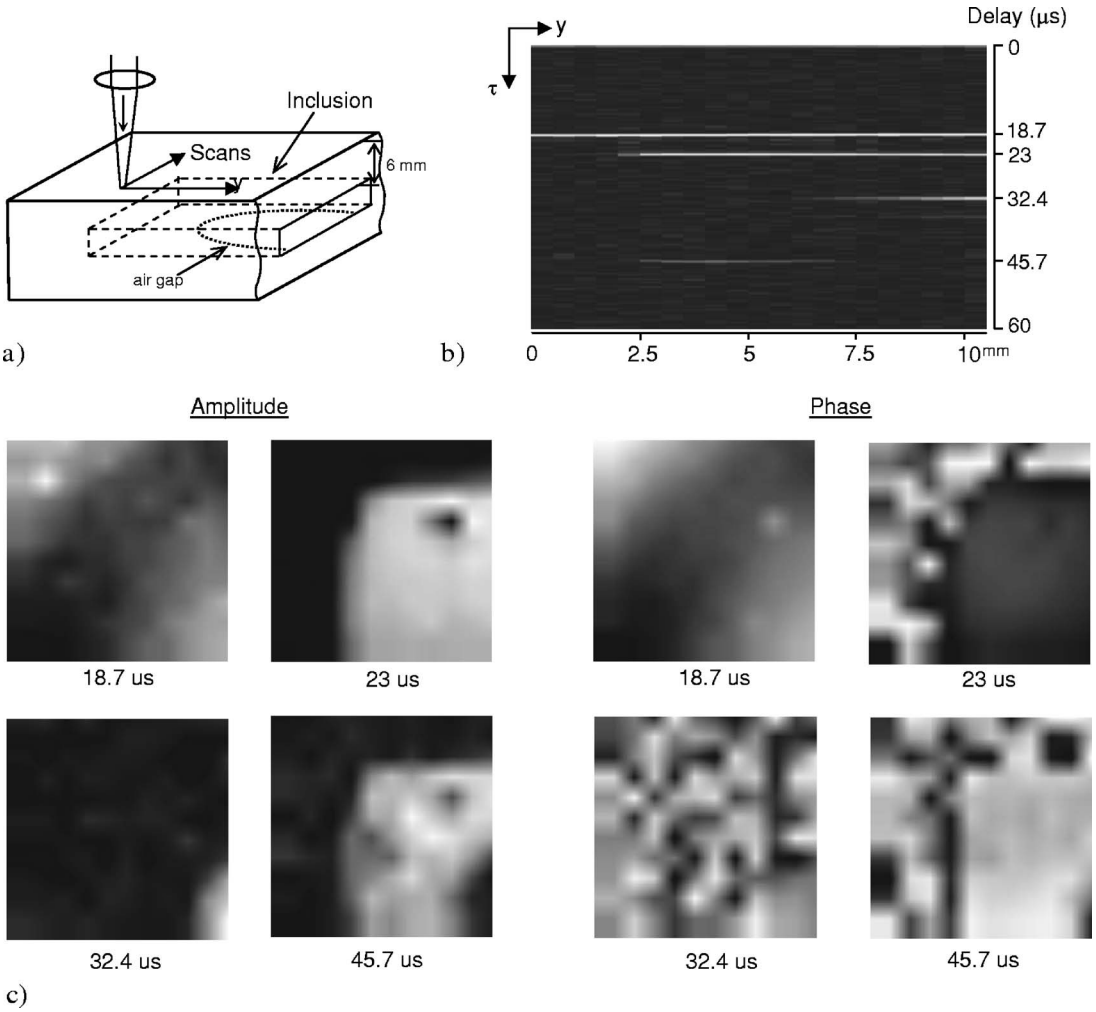

Fig. 4 FD-PTA depth-profilometric imaging of turbid plastisol phantoms. (a) Schematic diagram of the sample internal structure; (b) two-dimensional slice image of the phantom; (c) depth-selective images of amplitude and phase selected from a 3-D subsurface image data array at specific delay times.

ultrasonic echo imaging and is visible in Fig. 4(b) at scan distances greater than 7 mm (τ=32.4 μs), where the air gap was formed. In conclusion, Figs. 4(a) and 4(b) demonstrate the depth-profilometric ability of Fourier-domain biophotoacoustics over the entire thickness of the sample. The single transducer detection scheme employed in the present FD-PTA system allows one to image distributions of acoustic sources in three dimensions after recording numerous depth scans over an extended area of the surface. Such depth-selective imaging experiments are the most important feature of Fourier-domain biophotoacoustics. They were conducted with the same turbid plastisol phantom and results are shown in Fig. 4(c) for specific values of the time-delay parameter τ. Both amplitude and phase images reveal a corner of the rectangular-shaped inclusion at delay time 23 μs (6 mm below the top surface). Since an acoustic echo is a mirror image of the source, the cross-sectional image at 45.7 μs resembles the shape of inclusion with an additional dark area at the low-right corner due to the air gap, which prevents acoustic wave propagation through the sample thickness. These studies have been extended to three-dimensional imaging using complete *x-y* scans over the entire thickness of the phantom as shown in Fig. 5. Here Fig. 5(a) is the same as Fig. 4(b), but for the labeling of the various acoustically active layers, which are schematically depicted in Fig. 5(b). The depth selective capabilities of FD-PTA subsurface imaging are clearly demonstrated in the reconstructed three-dimensional image of Fig. 5(c). It should be noted that the presence of the airgap slice "C" below the layer "B" that generates echo "D" represents a high-impedance interface for the echo acoustic wave, which manifests itself as a shadow of layer C projected onto layer "D," exactly as imaged in Fig. 4(c).

To assess the capabilities of the FD-PTA method for imaging real tissue *ex-vivo*, chicken breasts were used as a suitable model of optical properties in human tissue. In order to simulate a tumor, disk-shaped plastisol inclusions (12 mm in diameter and 4 mm thick) with absorption coefficient μ_a =4 cm^{-1} were inserted into tissue specimens at various depths. Amplitude images of FD-PTA signals recorded in two chicken breast samples are shown in Fig. 6. The first specimen (Fig. 6(a)) contained an inclusion at the depth of 6 mm

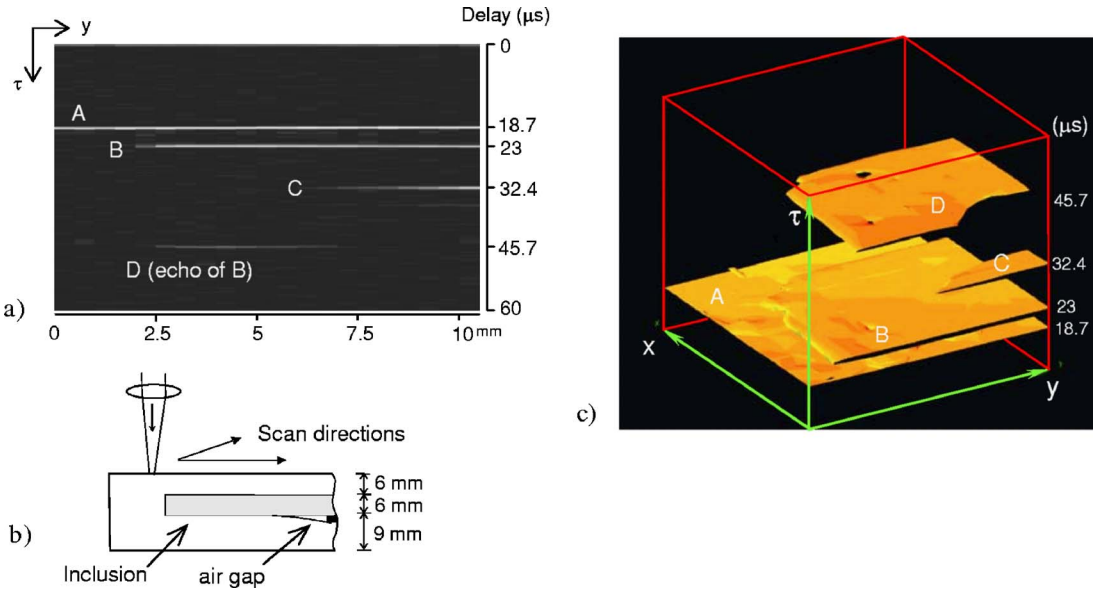

Fig. 5 (a) FD-PTA depth image of a planar light-absorbing inclusion (μ_a=4.2 cm^{-1}) embedded in a test plastisol phantom (μ_s'=1.3 cm^{-1}, μ_a =0.5 cm^{-1}) and scanning geometry (b) labels on the image indicate: A—phantom surface, B—top surface of the inclusion, C—artificial air gap under the inclusion, and D—acoustic echo of the top surface. (c) amplitude of two-dimensional scan across the surface resulting in a three-dimensional depth-selective image.

and was scanned with the laser beam along a straight line. Additionally, two black ink markers (M) were placed on the tissue surface to indicate its position. This 2-D image clearly shows the position of the surface markers and the signal from the subsurface inclusion at τ=21.5 μs. The second specimen had two inclusions (I) inserted at depths 3 mm and 7 mm with a lateral space of 5 mm between them. Again, a single line scan was recorded and the 2-D slice image is shown in Fig. 6(b), where the inclusions are indicated with arrows along with the surface marker (M). Both simulated tumors can be identified and their depth can be determined from the measured delay time of the correlation function peak and the speed of sound in tissue.

As seen in Fig. 5(c), scanning the laser beam with the ultrasonic transducer over a two-dimensional area can produce three-dimensional images of PTA sources in tissue. Similar to phantom experiments, 3-D volumetric data were recorded for chicken breast with a subsurface inclusion (Fig. 7(a)) and individual time-delay depth-selective images are shown in Figs. 7(b)–7(d). The sequence of the three PTA images shown in the figure was obtained at delay time τ =18.9 μs (amplitude only) corresponding to the mean depth of the black ink line, and at 21.6 μs, corresponding to the mean depth of the plastisol inclusion. The complete time-depth separation of the two features, which are superposed in the same lateral coordinate range, is very clear and is similar to the images shown in Fig. 4(c). The amplitude image of the inclusion, however, carries a superposed image of the black line, because the PTA amplitude is a function of the incident laser intensity, which is compromised through excess optical absorption along the line of the black ink marker. On the other hand, the phase image of the inclusion does not show the

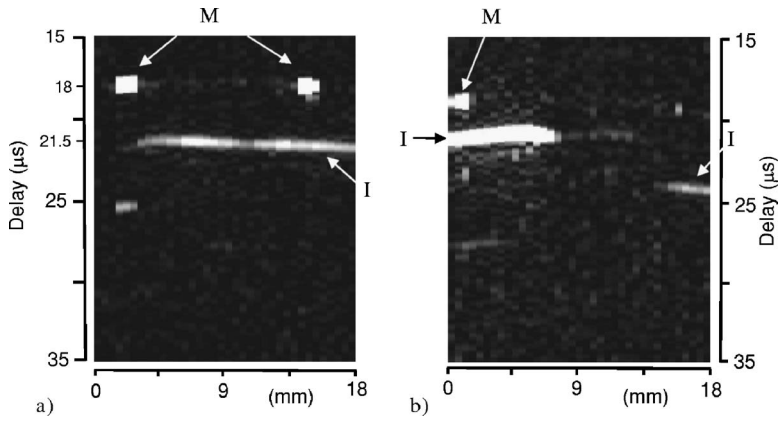

Fig. 6 Two-dimensional slice images of *ex-vivo* chicken breast samples with embedded inclusions (M—black ink marker, I—inclusion). (a) Single inclusion positioned 6 mm below the surface; (b) two discrete inclusions at the depths 3 mm and 7 mm.

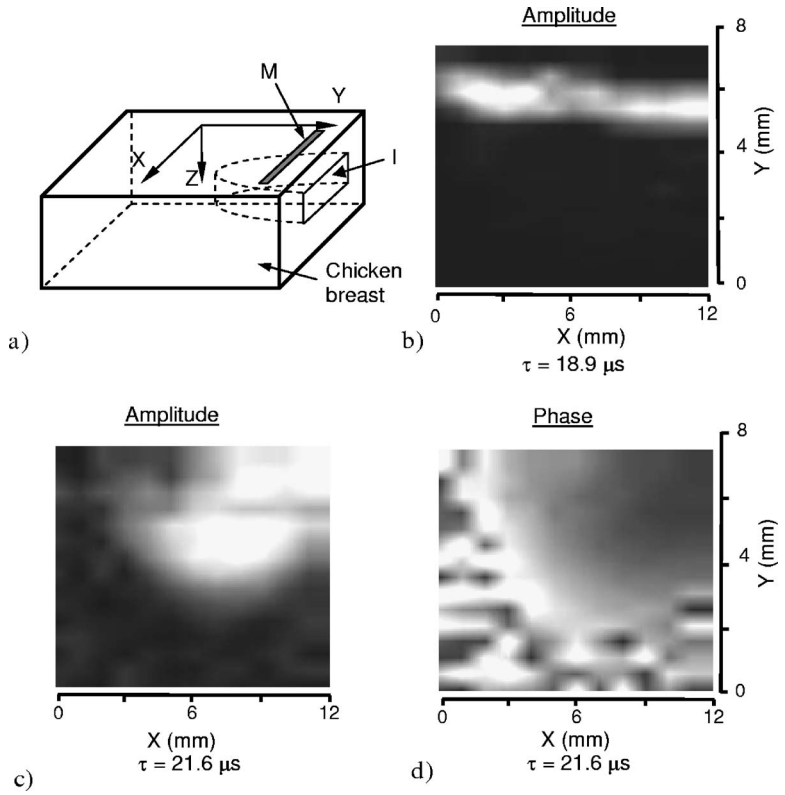

Fig. 7 Three-dimensional FD-PTA imaging of chicken breast with a disc-shaped subsurface inclusion. (a) Schematic of sample structure; (b) image of PTA amplitude at the delay time corresponding to the surface position; depth-selective images of amplitude (c) and phase (d) for the PTA signals generated from the subsurface inclusion.

black ink line: phase is independent of the intensity of the incident laser radiation as a ratio of the quadrature and in-phase signals and as such it construes a "true" photoacoustic image, independent of the optical properties of the surface. This characteristic property of frequency-domain fields has been reported in thermal-wave nondestructive imaging almost a quarter of a century ago,[19] but has not found its biophotoacoustics imaging analog until now. It is concluded that depth-selective PTA phase imaging can be a very important biomedical diagnostic tool, as it only depends on the local subsurface properties of the scanned sample (optical, thermal, and acoustic), but not on optical beam intensity modification due to the presence of overlaying absorbing structures and/or laser power fluctuations. This is a feature worth investigating in greater detail in the future. The apparent structure in the $\tau=21.6$ μs phase image of Fig. 7 is due to noise, as the absence of PTA signal outside the absorbing region at that depth (dark space in the amplitude image) renders the phase channel unstable. The noise can be easily filtered out using a simple algorithm that sets the phase equal to an appropriate value characteristic of the phase background.

Our studies are currently being extended to quantify limitations of the FD-PTA technique for imaging of deeper inclusions. An example of a single point depth-profilometric measurement of a chicken breast sample with inclusions positioned 9 mm and 17 mm below the surface are shown in Figs. 8(a) and 8(b), respectively. The data in Fig. 8(a) show two strong peaks (from the tissue surface and the shallow inclusion) with magnitude exceeding the noise floor by a factor of 4. Figure 8(b) was recorded using an ultrasonic transducer with sensitivity peak at 0.5 MHz and laser modulation sweeps in the range 0.1–1 MHz. Although imaging with low-frequency chirps reduces axial resolution, the depth of focus of the transducer is longer allowing detection of the deep inclusion.

4 Confocal Fourier-Domain Biophotoacoustics

Our ability to focus the ultrasonic transducer vertically in order to select acoustic responses from a small area confined to the focal spot by using the signal processing algorithm described in Sec. 2.2 allows us to implement confocal FD-PTA imaging, another form of depth-selective biophotoacoustics. According to Eq. (4), the heterodyne down-shifting of the LFM acoustic response relates the signal spectrum to the depth of PTA sources. To analyze the spectrum with high SNR, a narrow-band lock-in processing algorithm can be used with a harmonic reference signal synthesized internally with the frequency $f_z=\beta z/c_a$ that matches the transducer focal distance F, i.e., $f_z=\beta F/c_a$. In our experiments, the frequency sweep rate was $\beta=4\times10^9$ Hz/s and the transducer focal distance was $F=25.4$ mm. Therefore, the acoustic signals arriving at the transducer from the focal spot have frequency $f_z=72.5$ kHz after heterodyne mixing and low-pass filtering. Setting the reference frequency of the internal oscillator to f_z and using a sufficiently long integration time to increase SNR, PTA images of tissue at specific depths can be recorded. Typically, fine frequency tuning is required to take into account

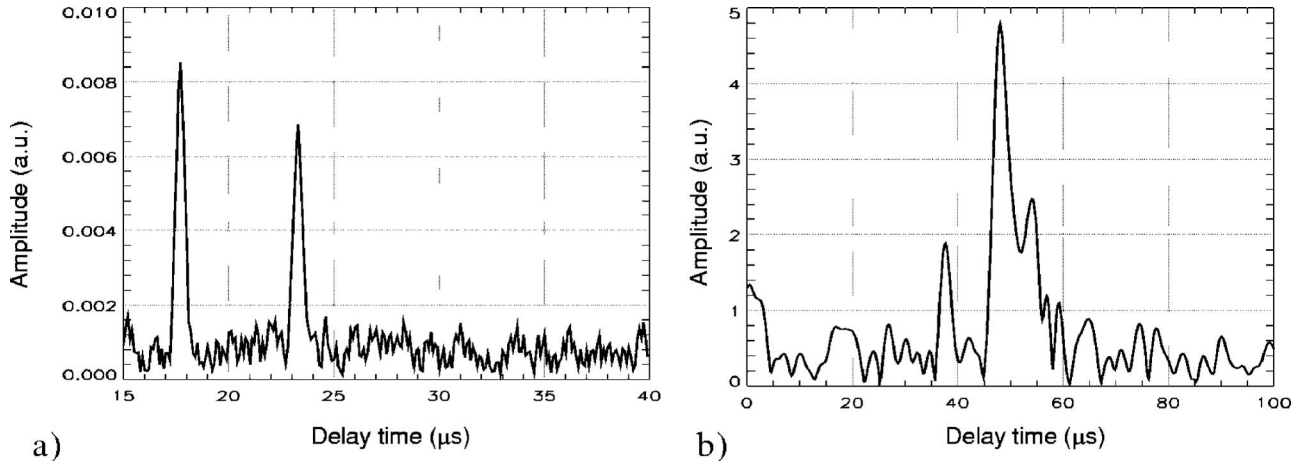

Fig. 8 Depth-profilometric measurements of subsurface inclusions in chicken breast positioned 9 mm (a) and 17 mm (b) deep. Laser modulation chirps were 1–5 MHz (a) and 0.1–1 MHz (b).

variations in the speed of sound. Figure 9 demonstrates an example of confocal biophotoacoustics imaging using a plastisol phantom with optical properties in the range of human tissue (μ_s'=3.1 cm^{-1} and μ_a=0.2 cm^{-1}) and with a subsurface inclusion (μ_a=4 cm^{-1}) positioned 7 mm below the surface. The test sample (Fig. 9(a)) was scanned horizontally while the transducer was aligned with its focal spot matched to that of the laser focal point (confocal) and both were positioned below the sample surface. Data were recorded continuously and processed in real time using software heterodyne mixing and lock-in detection at the fixed reference frequency of 72.4 kHz. Plots in Figs. 9(b) and 9(c) show amplitude and phase of the PTA signal along the line scan. Increasing of amplitude with simultaneous stabilization of the phase reading was observed when the laser beam confocal with the acoustic transducer traveled across the subsurface inclusion. The features disappeared completely if the internal oscillator was tuned to a different frequency or the transducer position with respect to sample was changed. Therefore, it was confirmed that the PTA signal originated at a specific depth in the sample. Using XY-scans, it is possible to record a two-dimensional image of the PTA response at the precisely controlled depth in tissue.

A valid comparison of the FD-PTA methodology with its pulsed counterpart will require similar conditions of laser excitation and detection. Nevertheless, a review of comparable results recorded using a single transducer[20] or a single transducer element within an array[21,22] demonstrates difficulties of the pulsed time-domain PTA method. Although theoretical estimates predict[6] imaging depth as high as 60 mm, the SNR of pulsed PTA measurements for subsurface inclusion depths greater than 20 mm decreases rapidly. The magnitude of the pulsed PTA signal from deeper tissue layers can be increased by raising the laser fluence, which results in significant increases of the background signal as well, or using a specific contrast agent[23] to enhance signal from specific chromophores. Our data demonstrate that FD-biophotoacoustics can provide a valuable alternative to pulsed methodologies. Inasmuch as the FD-PTA technique preserves the time-of-flight versus depth relationship, it can be implemented directly in pulsed PTA systems that utilize multi-element trans-

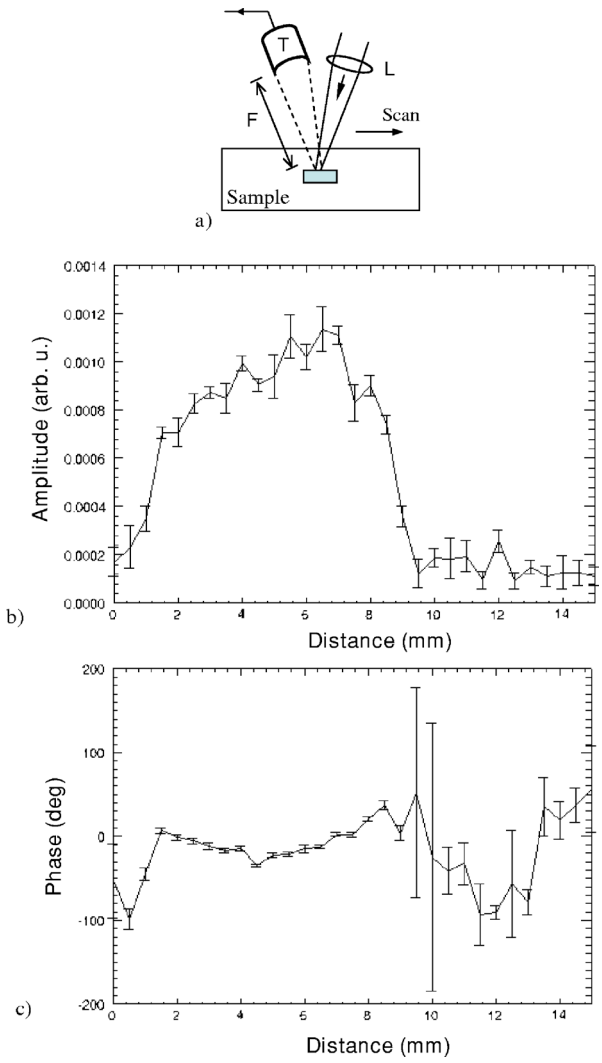

Fig. 9 Confocal FD-PTA imaging of tissue with a LFM laser excitation and lock-in signal processing. (a) Sample configuration (plastisol phantom with a subsurface inclusion), where T—transducer, L—lens, and F—the transducer's focal distance; plots of amplitude (b) and phase (c) recorded along a line scan.

ducer arrays and reconstruction algorithms for tomographic imaging of tissue. Additional motivation for further development of the FD-PTA methodology as a unique depth-selective imaging technique is provided by modern laser technology in the form of the availability of inexpensive laser sources with a wide range of wavelengths in the near-IR.

5 Conclusions

Fourier-domain biophotoacoustics depth-selective imaging based on frequency-swept optical excitation and frequency-domain coherent PTA detection and signal processing was introduced. This methodology offers an alternative approach to conventional pulsed photoacoustic imaging, combining simplicity of the pulsed time-of-flight measurements with highly sensitive coherent detection attributed to frequency-domain techniques. Two detection algorithms based on correlation signal processing and heterodyne mixing with lock-in demodulation were described. Our experiments with turbid phantoms and *ex-vivo* chicken breast specimens demonstrate the principle of FD-PTA imaging and reveal amplitude and phase imaging capabilities obtained with our system. Biophotoacoustic depth-selective imaging can be used to perform subsurface slice-by-slice image reconstruction from operator-determined, precisely controlled depths. Frequency-domain PTA with a linear frequency-swept laser source and heterodyne detection provides depth localization of subsurface tissue chromophores with resolution <1 mm and signal-to-noise ratio sufficient for noninvasive imaging in tissue 2 cm deep or better with a single transducer element. FD-PTA can be used to perform a single-point profilometric measurement as well as 2-D and 3-D imaging at precisely controlled depths (depth selectivity). It may be applicable to biomedical imaging of blood-rich tissue as in the case of subsurface cancerous tumors. Further improvements in the system may include application of detector arrays for signal acquisition, multiwavelength modulated optical excitation for chromophore specific imaging, advanced signal processing via spectral conditioning, and use of sophisticated modulation waveforms to increase SNR, and implementation of reconstruction algorithms for photothermoacoustic tomography of tissue.

Acknowledgments

The support of the Natural Sciences and Engineering Research Council of Canada (NSERC) through a CHRP grant is gratefully acknowledged. We wish to acknowledge Gloria Spirou for providing tissue phantoms used for the experiments reported in this paper.

References

1. A. A. Oraevsky, E. V. Savateeva, S. V. Solomatin, A. A. Karabutov, V. G. Andreev, Z. Gatalica, T. Khamapirad, and P. M. Henrichs, "Optoacoustic imaging of blood for visualization and diagnostics of breast cancer," *Proc. SPIE* **4618**, 81–94 (2002).
2. T. Khamapirad, P. M. Henrichs, K. Mehta, T. G. Miller, A. T. Yee, and A. Oraevsky, "Diagnostic imaging if breast cancer with LOIS: Clinical feasibility," *Proc. SPIE* **5697**, 35–44 (2005).
3. G. Ku, X. Wang, X. Xie, G. Stoica, and L. V. Wang, "Imaging of tumor angiogenesis in rat brains in vivo by photoacoustic tomography," *Appl. Opt.* **44** (5), 770–775 (2005).
4. A. Oraevsky, S. Jacques, and F. Tittel, "Measurement of tissue optical properties by time-resolved detection of laser-induced transient stress," *Appl. Opt.* **36** (1), 402–415 (1997).
5. A. A. Karabutov and A. A. Oraevsky, "Time-resolved detection of optoacoustic profiles for measurements of optical energy distribution in tissues," in *Handbook of Optical Biomedical Diagnostics*, V. V. Tuchin, Ed., Chap. 10, pp. 585–646, SPIE Press, Bellingham, WA (2002).
6. V. G. Andreev, A. A. Karabutov, S. V. Solomatin, E. V. Savateeva, V. Aleynikov, Y. V. Zhulina, R. D. Fleming, and A. A. Oraevsky, "Optoacoustic tomography of breast cancer with arc-array-transducer," *Proc. SPIE* **3916**, 36–47 (2000).
7. R. A. Kruger and W. L. Kiser, Jr., "Thermoacoustic CT of the breast: Pilot study observations," *Proc. SPIE* **4256**, 1–5 (2001).
8. C. G. A. Hoelen, F. F. M. de Mul, R. Pongers, and A. Dekker, "Three-dimensional photoacoustic imaging of blood vessels in tissue," *Opt. Lett.* **23** (8), 648–650 (1998).
9. C. G. A. Hoelen and F. F. M. de Mul, "Image reconstruction for photoacoustic scanning of tissue structures," *Appl. Opt.* **39** (31), 5872–5883 (2000).
10. Y. Fan, A. Mandelis, G. Spirou, I. A. Vitkin, and W. M. Whelan, "Laser photothermoacoustic heterodyned lock-in depth profilometry of turbid tissue phantoms," *Phys. Rev. E* **72** 051908 (2005).
11. Y. Fan, G. Spirou, A. Mandelis, and I. A. Vitkin, "Laser photothermoacoustic frequency-swept heterodyned lock-in depth profilometry for three-dimensional subsurface tissue imaging," *J. Acoust. Soc. Am.* **116**, 3523–3533 (2004).
12. M. I. Skolnik, ed., *Radar Handbook*, McGraw-Hill, New York (1990).
13. A. F. Fercher, C. K. Hitzenberger, G. Kamp, and S. Y. El-Zaiat, "Measurement of intraocular distances by backscattering spectral interferometry," *Opt. Commun.* **117**, 43–48 (1995).
14. G. Hausler and M. W. Lindner, "Coherence radar and spectral radar—new tools for dermatological diagnosis," *J. Biomed. Opt.* **3** (1), 21–31 (1998).
15. M. A. Choma, M. V. Sarunic, C. Yang, and J. A. Izatt, "Sensitivity advantage of swept source and Fourier domain optical coherence tomography," *Opt. Express* **11** (18), 2183–2188 (2003).
16. R. Leitgeb, C. K. Hitzenberger, and A. F. Fletcher, "Performance of Fourier domain vs. time domain optical coherence tomography," *Opt. Express* **11** (8), 889–894 (2003).
17. E. C. Farnett and G. H. Stevens, "Pulse compression radar," in *Radar Handbook*, M. I. Skolnik, Ed., Chap. 10, McGraw-Hill, New York (1990).
18. G. M. Spirou, A. A. Oraevsky, I. A. Vitkin, and W. M. Whelan, "Optical and acoustic properties at 1064 nm of polyvinyl chloride-plastisol for use as a tissue phantom in biomedical optoacoustics," *Phys. Med. Biol.* **50** (14), N141–N153 (2005).
19. G. Busse, "Optoacoustic and photothermal material inspection techniques," *Appl. Opt.* **21**, 107–110 (1982).
20. R. O. Esenaliev, A. A. Karabutov, and A. A. Oraevsky, "Sensitivity of laser opto-acoustic imaging in detection of small deeply embedded tumors," *IEEE J. Sel. Top. Quantum Electron.* **5** (4), 981–988 (1999).
21. S. Manohar, A. Kharine, J. C. G. van Hespen, W. Steenbergen, F. M. de Mul, and T. G. van Leeuwen, "Photoacoustic imaging of inhomogenities embedded in breast tissue phantoms," *Proc. SPIE* **4960**, 64–75 (2003).
22. S. Manohar, A. Kharine, J. C. G. van Hespen, W. Steenbergen, and T. G. van Leeuwen, "Photoacoustic mammography laboratory prototype: Imaging of breast tissue phantoms," *J. Biomed. Opt.* **9** (6), 1172–1181 (2004).
23. G. Ku and L. V. Wang, "Deeply penetrating photoacoustic tomography in biological tissues enhanced with an optical contrast agent," *Opt. Lett.* **30** (5), 507–509 (2005).